tvst

Article

Effects of Valproic Acid and Mitomycin C Combination Therapy in a Rabbit Model of Minimally Invasive Glaucoma Surgery

Li-Fong Seet[1,3,*], Zhu Li Yap[1–4,*], Stephanie W. L. Chu[1], Li Zhen Toh[1], Farah Ilyana Ibrahim[4], Xiao Teng[5], and Tina T. Wong[1–4]

[1] Singapore Eye Research Institute, Singapore
[2] Department of Ophthalmology, Yong Loo Lin School of Medicine, National University of Singapore, Singapore
[3] Duke-NUS Medical School Singapore, Singapore
[4] Singapore National Eye Centre, Singapore
[5] HistoIndex Pte. Ltd., Singapore

Correspondence: Li-Fong Seet, Singapore Eye Research Institute, 20 College Road, The Academia, Discovery Tower, #06-98, Singapore 169856, Singapore.
e-mail: seet.li.fong@seri.com.sg
Tina T. Wong, Singapore National Eye Centre, 11 Third Hospital Avenue, Singapore 168751, Singapore.
e-mail: tina.wong.t.l@singhealth.com.sg

Received: August 12, 2021
Accepted: November 29, 2021
Published: January 19, 2022

Keywords: Collagen; fibrosis; glaucoma; MIGS; mitomycin C; surgery; valproic acid; VEGF

Citation: Seet LF, Yap ZL, Chu SWL, Toh LZ, Ibrahim FI, Teng X, Wong TT. Effects of valproic acid and mitomycin C combination therapy in a rabbit model of minimally invasive glaucoma surgery. Transl Vis Sci Technol. 2022;11(1):30, https://doi.org/10.1167/tvst.11.1.30

Purpose: This study aimed to compare the effectiveness of combination therapy consisting of low-dose mitomycin C (MMC) and valproic acid (VPA) against high-dose MMC for improving the scar phenotype in minimally invasive glaucoma surgery (MIGS).

Methods: A rabbit model of MIGS incorporating the PreserFlo MicroShunt was treated with high (0.4 mg/mL) or low (0.1 mg/mL) doses of MMC or with combination therapy consisting of low-dose (0.1 mg/mL) MMC and VPA. Operated eyes were examined by live ocular imaging, histochemical evaluation, multiphoton quantitation of collagen characteristics, and molecular analyses.

Results: Although high-dose MMC obliterated the vasculature, combination therapy vastly improved the postoperative tissue morphology by maintaining the vasculature without increased vascularization. Combination therapy also altered collagen morphology and reduced encapsulation of the MicroShunt distal end, which remained at risk with MMC treatment alone. Multiphoton quantitation indicated that the combination therapy significantly reduced collagen density and fiber dimensions compared with monotherapy. At the molecular level, combination therapy significantly reduced *Vegfa*, *Vegfc*, and *Vegfd* expression and inhibited *Col1a1* upregulation from baseline levels, all of which low-dose MMC alone was unable to achieve. Notably, COL1A1 protein levels appeared more consistently suppressed by combination therapy compared with high-dose MMC alone.

Conclusions: Compared with high-dose MMC, combination therapy was less toxic by sparing the vasculature and potentially more effective in reducing scarring via the regulation of collagen content and organization.

Translational Relevance: VPA may be combined with low-dose MMC to replace high-dose MMC to deliver safe and effective anti-scarring outcomes.

Introduction

Glaucoma is an irreversible optic neuropathy and elevated intraocular pressure (IOP) is the main risk factor. Reducing IOP is the only known effective modifiable factor in managing and preventing glaucoma progression.[1] The current gold standard for providing the most reliable IOP reduction is through glaucoma filtration surgery (GFS). In recent years, surgical options for glaucoma therapy, which include the use of glaucoma drainage devices (GDDs),[2] have further diversified with the introduction of minimally invasive glaucoma surgery (MIGS). These surgeries aim to reduce IOP in a safer and less traumatic manner compared with traditional GFS or GDDs.[3] The

Preserflo MicroShunt (Santen Pharmaceutical Company, Osaka, Japan) operates on a mechanism similar to a GDD as it drains aqueous humor into the subconjunctival space via a shunt.[4] The 8.5-mm-long MicroShunt with a lumen diameter of 70 µm is made of a stable and flexible polymer and implanted via an ab externo approach. To reduce the risk of fibrosis, the procedure requires augmentation with intraoperative application or injection of mitomycin C (MMC).[5]

The primary mechanism of MMC action is via DNA alkylation and formation of DNA cross-links, preventing DNA synthesis leading to cell-cycle arrest, as well as cell death through apoptosis. Indeed, single exposures to MMC have been shown to induce profound long-term inhibition of proliferation and apoptosis of human conjunctival fibroblasts.[6] These findings have led to the successful clinical use of MMC as an adjuvant in glaucoma filtration surgery[7] and more recently in MIGS.[8] However, MMC is associated with cytotoxic effects. We have demonstrated that a one-time exposure to MMC caused persistent signs of apoptosis in the conjunctival epithelium in a mouse model of conjunctival scarring at 28 days post-treatment.[9] The risk of conjunctival epithelium breakdown is therefore high and likely explains the reported serious complications associated with MMC application such as bleb leaks, hypotony, and endophthalmitis.[10,11] On the other hand, growth-arrested human Tenon's fibroblasts following single exposures to MMC have been demonstrated to retain the capacity to express major scar proteins such as type I collagen and migrate chemotactically.[12,13] The latter deficiency may explain why surgeries continue to fail despite the use of MMC.[14] Hence, although MMC is still regarded as the gold-standard treatment to reduce scar formation after GFS and GDD implantation, there is the risk of vision-threatening complications and the possibility that scarring may still occur in the long term due to its limited effects on other wound healing responses.

To reduce the risk of adverse effects due to MMC, multiple studies have suggested that MMC concentrations may be adjusted.[15] In ophthalmic surgery, MMC is used in concentrations ranging from 0.1 to 0.5 mg/mL.[16] At the most commonly used concentration range from 0.2 to 0.4 mg/mL, multiple adverse effects were reported following GFS.[17] At 0.1 mg/mL, MMC was reported to be significantly less effective in managing IOP compared with 0.4 mg/mL,[18] but it was thought to be safer and caused fewer complications.[15,19,20] Hence, to improve low-dose MMC efficacy, combining it with other therapeutics or therapy has been proposed, but none of these combinations has been generally accepted or widely used in clinical practice.[17]

Valproic acid (VPA) is a small molecule drug widely used for the treatment of neurological disorders, with potential efficacy for numerous diseases, including fibrotic disorders.[21] We have demonstrated that VPA was effective in reducing collagen production in a mouse model of conjunctival scarring and a rabbit model of MIGS.[22,23] We hypothesize that the capacity of VPA to modulate type I collagen expression via selective regulation of Smads[22] will complement the anti-metabolite activity of MMC and help provide improved reduction of fibrosis after GFS or MIGS. In this study, we compared the effectiveness of a combination therapy of VPA and low-dose MMC at 0.1 mg/mL (MMC+VPA) against that of low-dose and high-dose MMC alone to regulate postoperative scarring responses in a rabbit model of MIGS implanted with the PreserFlo MicroShunt.

Methods

Rabbit Model of MIGS

All animal experiments were approved by the Institutional Animal Care and Use committee and treated in accordance with the ARVO Statement on the Use of Animals in Ophthalmic and Vision Research. A total of 15 NZW rabbits, five per treatment condition, were used in this study. The rabbits, 12 to 14 weeks old and weighing 2 to 2.4 kg, were acclimatized for 7 days before surgery at the SingHealth Experimental Medical Centre (Singapore General Hospital, Singapore). The surgical procedure involving the Santen PreserFlo MicroShunt was performed in the rabbit as previously described.[23] MMC was applied via a surgical sponge soaked in either 0.4 mg/mL (high-dose) or 0.1 mg/mL (low-dose) solution. The sponge was placed within the conjunctival/Tenon's flap for 2 minutes before removal, then carefully and rigorously rinsed with 10 to 20 mL of saline solution, followed by insertion of the MicroShunt as per the manufacturer's instructions. Immediately after suturing, the MMC-treated eyes were subjected to one subconjunctival injection of 0.1 mL PBS for the arms indicated as high-dose MMC or low-dose MMC alone, or with 0.1 mL VPA at 300 µg/mL for the arm indicated as low-dose MMC+VPA. One drop of guttae chloramphenicol and Betnesol-N (Glaxo Wellcome, Uxbridge, UK) ointment was instilled at the end of the procedure. Only the left eye of each rabbit was operated on, and the surgical procedure was performed at the same site superiorly in each animal. Follow-up subconjunctival injections of PBS or VPA at the same volume and concentration were given at the following

postoperative time points: days 1, 2, 3, 4, 5, 6, 7, 10, 14, and 21. Topical antibiotic and steroid drops were administered daily in both groups for 3 weeks after the experimental surgery. The animals were sacrificed on day 28 and eyes enucleated for analyses.

Live Imaging of Rabbit Eyes

Postoperative assessments by unmasked observers were performed at weekly intervals for 4 weeks before sacrifice. Rabbits were anesthetized before imaging was performed. Slit-lamp biomicroscopy was performed using a Righton LED Slit Lamp MW50D (Right Mfg. Co., Ltd., Tokyo, Japan). In vivo confocal microscopic examinations of blebs were performed using an HRT3 confocal scanning laser microscope (Heidelberg Engineering, Heidelberg, Germany).

Histochemical Evaluation

After euthanasia on day 28, the eye was dissected, fixed with paraformaldehyde, and placed in optimal cutting temperature compound in a cryomold before freezing in dry ice and storage at −80°C. Then, 5 µm cryosections were prepared using a Zeiss Microm HM550 (Carl Zeiss Meditec, Jena, Germany) and then examined by histochemical analyses. Staining with hematoxylin and eosin (H&E) or picrosirius red was performed as described previously.[23] The Masson's Trichrome Stain Kit was purchased from Electron Microscopy Sciences (Hatfield, PA) and used according to the manufacturer's instructions. Polarization microscopy for picrosirius red–stained cryosections was performed using an ECLIPSE Ti Series microscope (Nikon Instruments, Melville, NY) as described before.[23] Evaluations were made by unmasked observers.

Multiphoton Imaging and Quantitative Analysis

Images of unstained cryosections were acquired on a fully automated, programmable, multiphoton imaging platform (Genesis 200; HistoIndex Pte. Ltd., Singapore) as described previously.[23] The HistoIndex FibroIndex software was used to analyze the region of interest in the images (https://www.histoindex.com/product-andservices/).[24] The distributions of collagen fiber morphometric traits, including density, reticulation, thickness, and length, were described by normalized quantitative fibrosis parameters.[24] Five independent rabbit eyes were examined for each condition, and three independent cryosections from each eye were imaged for quantitative analyses.

Real-Time Quantitative Polymerase Chain Reaction

For mRNA analyses of the rabbit model, a small portion of the operated conjunctiva was excised upon euthanasia on day 28. A similar area of unoperated conjunctiva in the contralateral eye of each rabbit was harvested to obtain baseline values to calculate fold changes in transcript expression. Rabbit conjunctival tissues were processed and analyzed by quantitative polymerase chain reaction (qPCR) as described previously.[23] qPCR reactions were performed in triplicate and run using the LightCycler 480 System (Roche Diagnostics, Indianapolis, IN). All mRNA levels were measured as cycle threshold (CT) levels. *Actb* was determined to be the most suitable housekeeping gene of the four analyzed (*Actb*, *Rna18s1*, *Gapdh*, and *Rpl13a*) using NormFinder software.[25] The value for each operated eye was calculated as a fold change relative to the corresponding contralateral unoperated eye by the $2^{-\Delta\Delta CT}$ method. Primers used were as follows: *Actb*-forward, 5′-ATCATGAAGTGCGACGTGGA-3′, and *Actb*-reverse, 5′-ATCTCCTTCTGCATGCGGTC-3′; *Vegfa*-forward, 5′- GAAGAAGGAGACAATAAACCC-3′, and *Vegfa*-reverse, 5′- ACCAGAGGCACGCAGGAA-3′; *Vegfc*-forward, 5′-CAAATGCTGGAGATGACTCTGC-3′, and *Vegfc*-reverse, 5′-TCGAGTTCTTTGTGGGGTCC-3′; *Vegfd*-forward, 5′-ACCACACAGGTTGTAAGTGCT-3′, and *Vegfd*-reverse, 5′-TTGAATTGGGAACAGCGGTC-3′; *Col1a1*-forward, 5′- CGATGGCTTCCAGTTCGAGT-3′, and *Col1a1*-reverse, 5′- GCTACGCTGTTCTTGCAGTG-3′. The *Vegfb* sequence is currently not available for the rabbit and was not analyzed.

Immunoblot Analysis

Operated conjunctival tissues were harvested after 28 days and processed as described previously.[26] Antibodies against collagen type I α 1 and glyceraldehyde-3-phosphate dehydrogenase (GAPDH) were purchased from Abnova Corporation (Taipei, Taiwan) and Santa Cruz Biotechnology (Santa Cruz, CA) respectively. Horseradish peroxidase–conjugated secondary antibodies were obtained from Jackson ImmunoResearch Laboratories (West Grove, PA). Densitometric quantitation was performed using Image Lab software version 6.0.1 (Bio-Rad Laboratories, Hercules, CA). Normalization to correct for

variations in loading was performed using GAPDH as the housekeeping protein.

Statistical Analysis

All data are expressed as mean ± standard deviation. Values for the respective activities under the indicated treatment conditions were calculated for significance of differences by one-way ANOVA with Bonferroni adjustments using SPSS Statistics 19 (IBM Corporation, Armonk, NY). Statistical significance was defined as $P < 0.05$.

Results

Effects of Combination Therapy on Bleb Vasculature

We have previously shown that VPA at 300 µg/mL was effective in significantly downregulating *Col1a1* expression in vitro in mouse and rabbit conjunctival fibroblasts and in vivo in mouse and rabbit models of conjunctival scarring and MIGS.[22,23] In this study, we compared the postoperative responses to treatments with high-dose (0.4 mg/mL) MMC, low-dose (0.1 mg/mL) MMC, and low-dose (0.1 mg/mL) MMC combined with 300 µg/mL VPA (MMC+VPA) in the rabbit model of MIGS described previously.[23] Although MMC was applied via surgical sponges, VPA was administered as subconjunctival injections over the course of 3 weeks. The postoperative blebs, wherein the tubular structures of the implants in the subconjunctival space under the Tenon's capsule may be observed by slit-lamp biomicroscopy (Figs. 1A–1C, arrows), were sustained for at least 28 days under all three conditions. However, the morphologies of the blebs differed among the treatment conditions. In the bleb treated with high-dose MMC, there was marked reduction in the superficial bleb vasculature in the focal area of treatment in the first week after surgery, which then further diminished with time, culminating in almost complete demarcation of the bleb from the surrounding untreated tissue (Figs. 1A, 1D, 1G, 1J). High-dose MMC also produced a cystic bleb with observable microcysts and pronounced elevation above the scleral bed (Fig. 1J). In the bleb treated with low-dose MMC, a mildly cystic bleb with a less defined boundary from normal tissue and a visibly smaller avascular area (Figs. 1E, 1H, 1K, asterisk) with apparent progressive return of vascularization was visualized (Figs. 1B, 1E, 1H, 1K, dotted box). In the bleb treated with MMC+VPA, normal vascularization traversing the entire area of the postoperative area was visualized, with no apparent increase in vascularization for at least 4 weeks with the combination therapy (Figs. 1C, 1F, 1I, 1L). These observations suggest that, although low-dose MMC was less deleterious on the vasculature compared with high-dose MMC, the incorporation of VPA resulted in the maintenance of vascularization in the postoperative conjunctiva.

Effects of Combination Therapy on Vasculature Morphology

In the epithelial layer of the day 28 bleb treated with high-dose MMC, live confocal microscopy revealed the presence of numerous hyporeflective spaces or microcysts that tended to be irregular in shape and size and so closely juxtaposed that they appeared to be clustered into large hyporeflective spaces (Fig. 2A, asterisk). In contrast, fewer, more regularly shaped and discrete microcysts were observed among the superficial conjunctival epithelial cells in blebs treated with low-dose MMC (Fig. 2B, asterisk) or MMC+VPA (Fig. 2C, asterisk). In the sub-Tenon's space, large, optically clear, and nonencapsulated cysts riddled the stromal connective tissue treated with high-dose MMC (Fig. 2D, asterisk). In contrast, the reticular stromal matrices of the blebs treated with low-dose MMC (Fig. 2E, asterisk) or MMC+VPA (Fig. 2F, asterisks) featured comparatively smaller microcysts. In the deeper pre-scleral and scleral hyperreflective plane, perfused blood vessels showing a variety of diameters, with some appearing markedly large, were present in blebs treated with high-dose MMC (Fig. 2G, arrowhead and arrows) or low-dose MMC (Fig. 2H, arrowheads and arrow). In comparison, blood vessels in the MMC+VPA–treated bleb often appeared to be finer in appearance (Fig. 2I, arrows). These observations suggest that the incorporation of VPA modifies vascular organization.

Effects of Combination Therapy on Postoperative Scar Collagen Organization

In the H&E–stained unoperated rabbit subconjunctiva, cells were observed in the midst of an extracellular matrix (ECM) network populated by a loosely organized array of fibers, with the most prominent fibers running parallel to the scleral plane (Fig. 3A). Treatment with high-dose MMC obliterated a substantial portion of the ECM structure, resulting in a large void where few or no fibers were detected (Fig. 3B, asterisk). At the top and bottom boundaries of this clear space were fibers with detectable cells, likely delineating the perimeter of contact with the high-dose

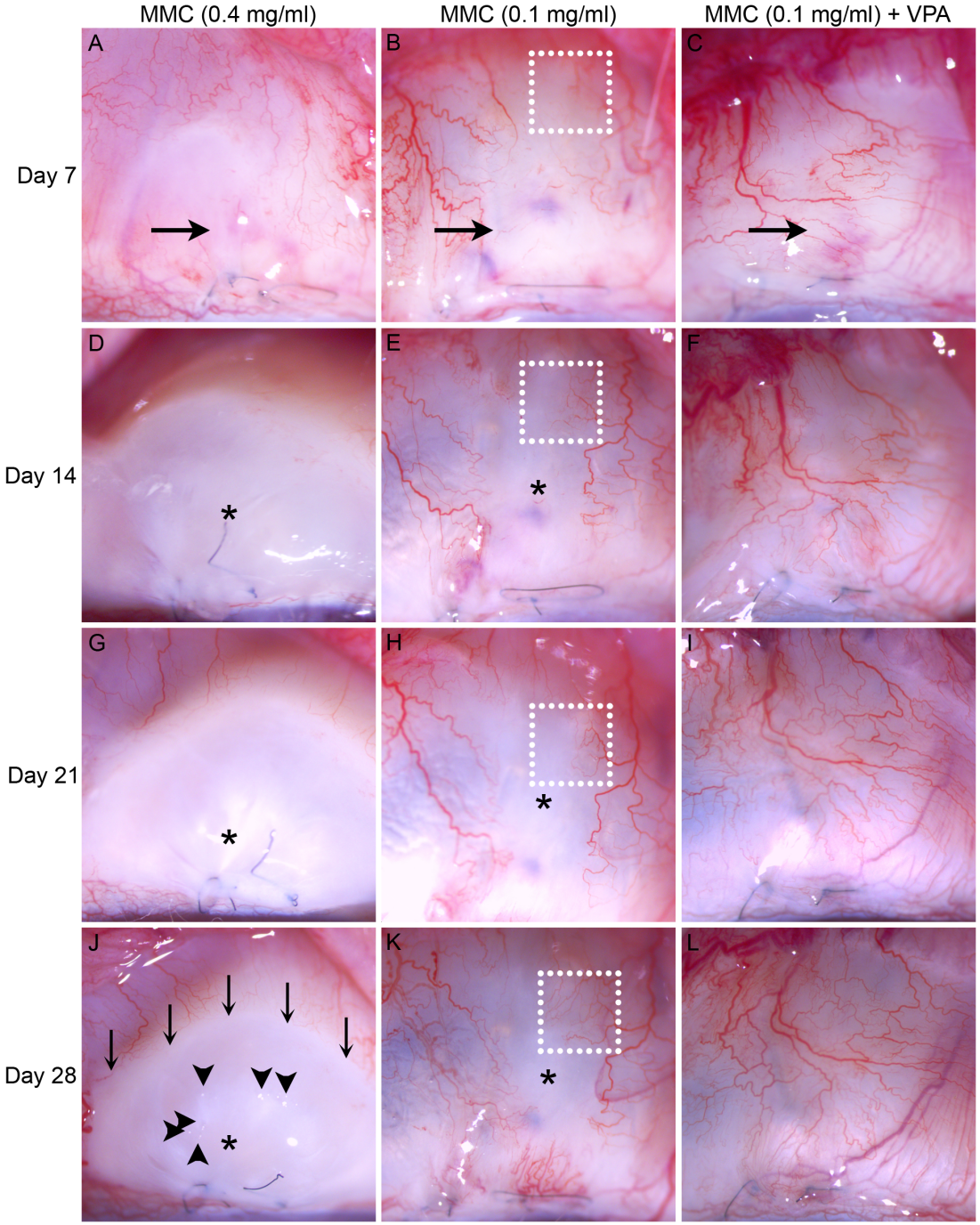

Figure 1. Slit lamp biomicroscopy of the postoperative conjunctivas in the rabbit model of MIGS. The same postoperative eye of each rabbit treated with high-dose (0.4 mg/mL) MMC, low-dose (0.1 mg/mL) MMC, or low-dose (0.1 mg/mL) MMC + 300 µg/mL VPA was imaged on a weekly basis from day 7 up to 28. The location of the MicroShunt in the subconjunctival space overlying the sclera is indicated by the *horizontal arrow*. Observable microcysts in the day 28 blebs are indicated by *arrowheads*. Apparent demarcation of the avascular bleb from normal tissue is indicated by *downward arrows*. *Asterisks* indicate avascular areas. The *dotted box* tracks the same area within the bleb treated with low-dose MMC to help visualize progressive vascularization over time.

MMC. In contrast, the ECM in the bleb treated with low-dose MMC retained a fibrous network that permeated throughout the matrix except for a few small areas of ECM-void spaces (Fig. 3C, asterisks). Co-treatment with VPA appeared to cause further changes to the ECM, as visualized fibers were visibly weaker staining

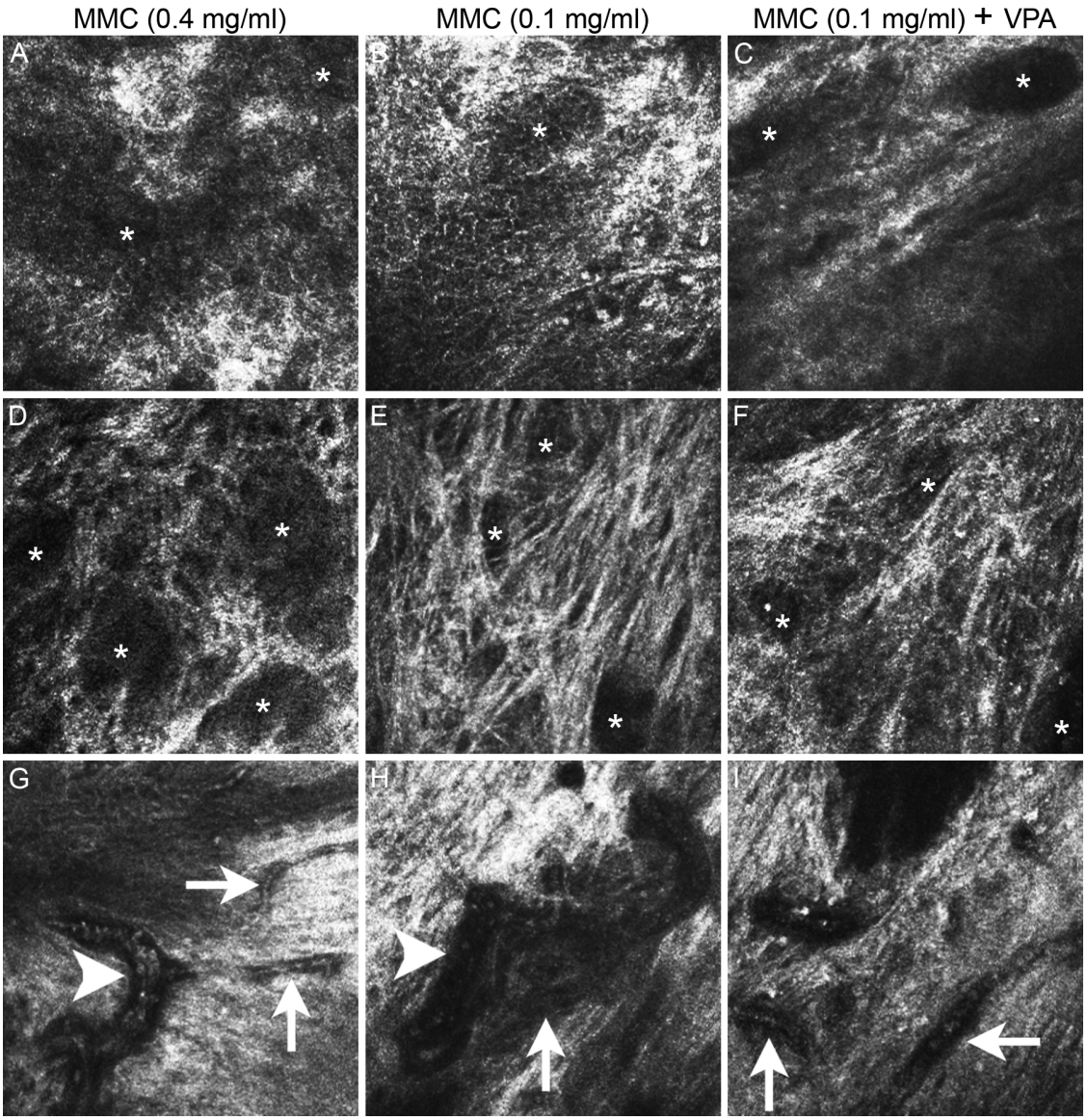

Figure 2. In vivo confocal microscopy of the day 28 postoperative conjunctivas. Rabbit eyes were treated as indicated. The postoperative blebs were imaged progressively from epithelial surface to the pre-scleral layer: conjunctival epithelium (A–C), stromal matrix (D–F), and pre-sclera and sclera layers (G–I). *Asterisks* indicate microcysts. Examples of thicker blood vessels are marked by *arrowheads* and thinner blood vessels by *arrows*.

and considerably more sparsely organized compared with those exposed to low-dose MMC monotherapy (Fig. 3D).

Further evaluation via Masson's trichrome staining revealed that the unoperated conjunctival stromal collagen network featured blue-staining fibers of variable thickness, with finer and shorter fibers immediately underneath the epithelium scattered in orientation, whereas thicker and longer fibers in the stromal matrix ran parallel to the scleral plane (Fig. 3E). The presence of a large collagen-void stroma was confirmed in the bleb treated with high-dose MMC (Fig. 3F, asterisk), whereas ECM remnants retained the organization reminiscent of the unoperated tissue. In the bleb treated with low-dose MMC, numerous fibers were detected throughout most of the stromal matrix except for a few small fiber-void areas (Fig. 3G, asterisk). However, the majority of the fibers were stained red/purple instead of the bona fide blue for mature collagen fibers (Fig. 3G). The weakest trichrome signals were visualized in the bleb treated with MMC+VPA (Fig. 3H). As the trichrome method is known to be

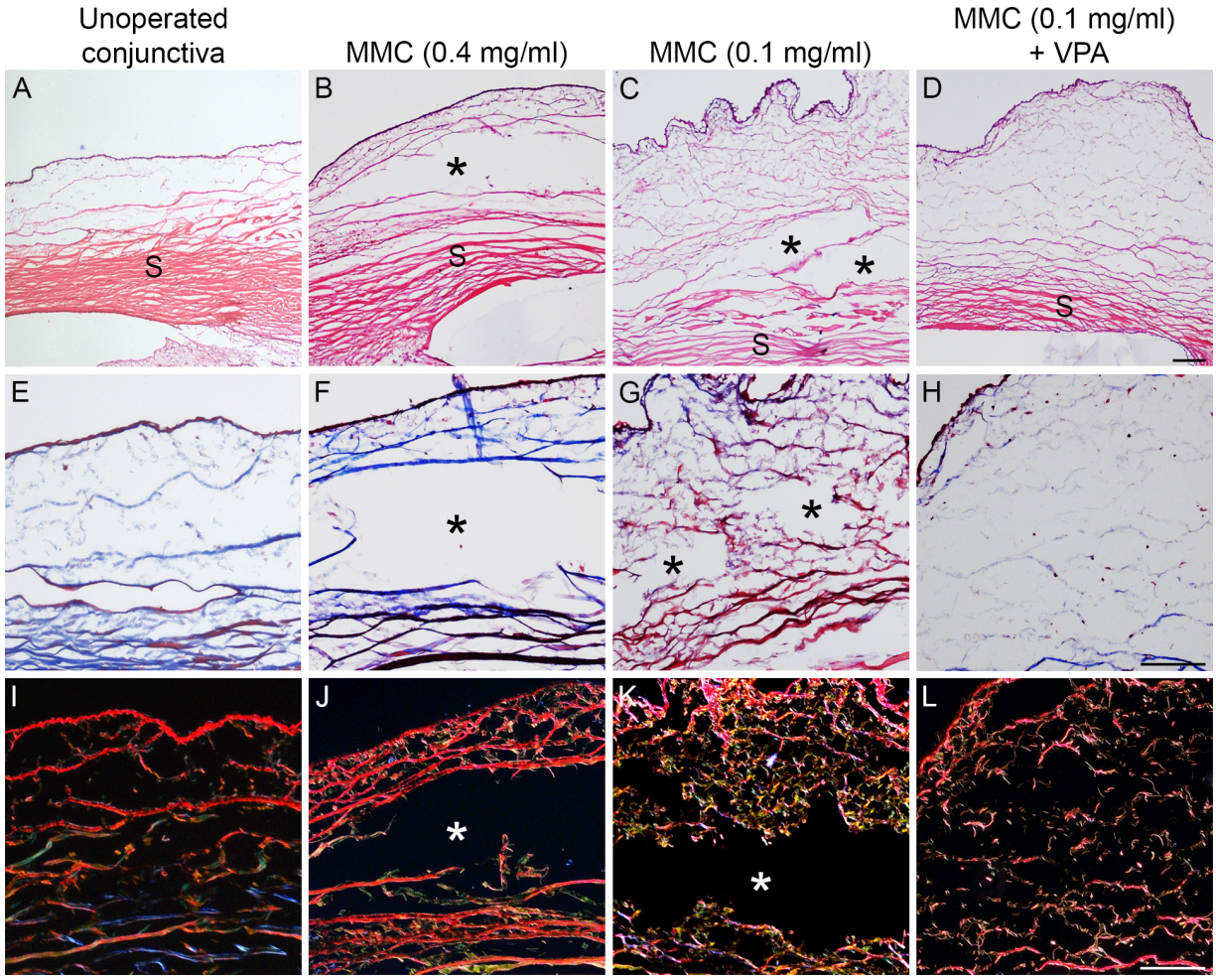

Figure 3. Histochemical evaluation of collagen characteristics in the day 28 postoperative conjunctivas. Rabbit eyes were treated as indicated. Unoperated normal rabbit conjunctiva is included for comparison. Serial frozen sections of the same eye were visualized via staining with H&E (A–D), Masson's trichrome (E–H), and picrosirius red (I–L). Panels (A) to (H) were viewed under light microscopy, and (I) to (L) were viewed via polarized microscopy. *Asterisks* indicate ECM-void spaces. S, sclera. *Scale bar*: 100 µm.

poor for very thin collagen fibers, it is possible that the weakly stained, or red/purple-stained, fibers indicate fine, delicate collagen fibers.

The polarized colors of picrosirius red–stained fibrillar collagen are dependent on fiber thickness and packing and may be used to differentiate thin, newly formed green/yellow collagen fibers from thick, mature, orange/red collagen bundles.[27] In the unoperated conjunctiva, the majority of the collagen fibers appeared as red mature fibers, whereas green/yellow collagen fibers were a minority (Fig. 3I). In the bleb treated with high-dose MMC, the majority of the collagen bundles surrounding the fiber-void area also appeared orange/red (Fig. 3J), supporting the notion that this area was spared from MMC contact. On the other hand, numerous fine green/yellow fibers dominated the stromal matrix of the bleb treated with low-dose MMC (Fig. 3K), suggesting that these fibers represent recently produced collagens with diminished fiber packing density and/ or reduced fiber size. On the other hand, predominantly orange/red collagen fibers reigned in the bleb treated with MMC+VPA; however, these fibers were conspicuously much finer and more scattered or disorganized compared with those in the unoperated conjunctiva (Fig. 3L). These data suggest that, although low-dose MMC appeared to allow active collagen synthesis, incorporation of the VPA disrupted both new collagen production and organization.

Effects of Combination Therapy on Microshunt Encapsulation

Poly(styrene-*b*-isobutylene-*b*-styrene) tubes were previously shown to induce only a modest and discontinuous collagen deposition at 3 and 6 months when

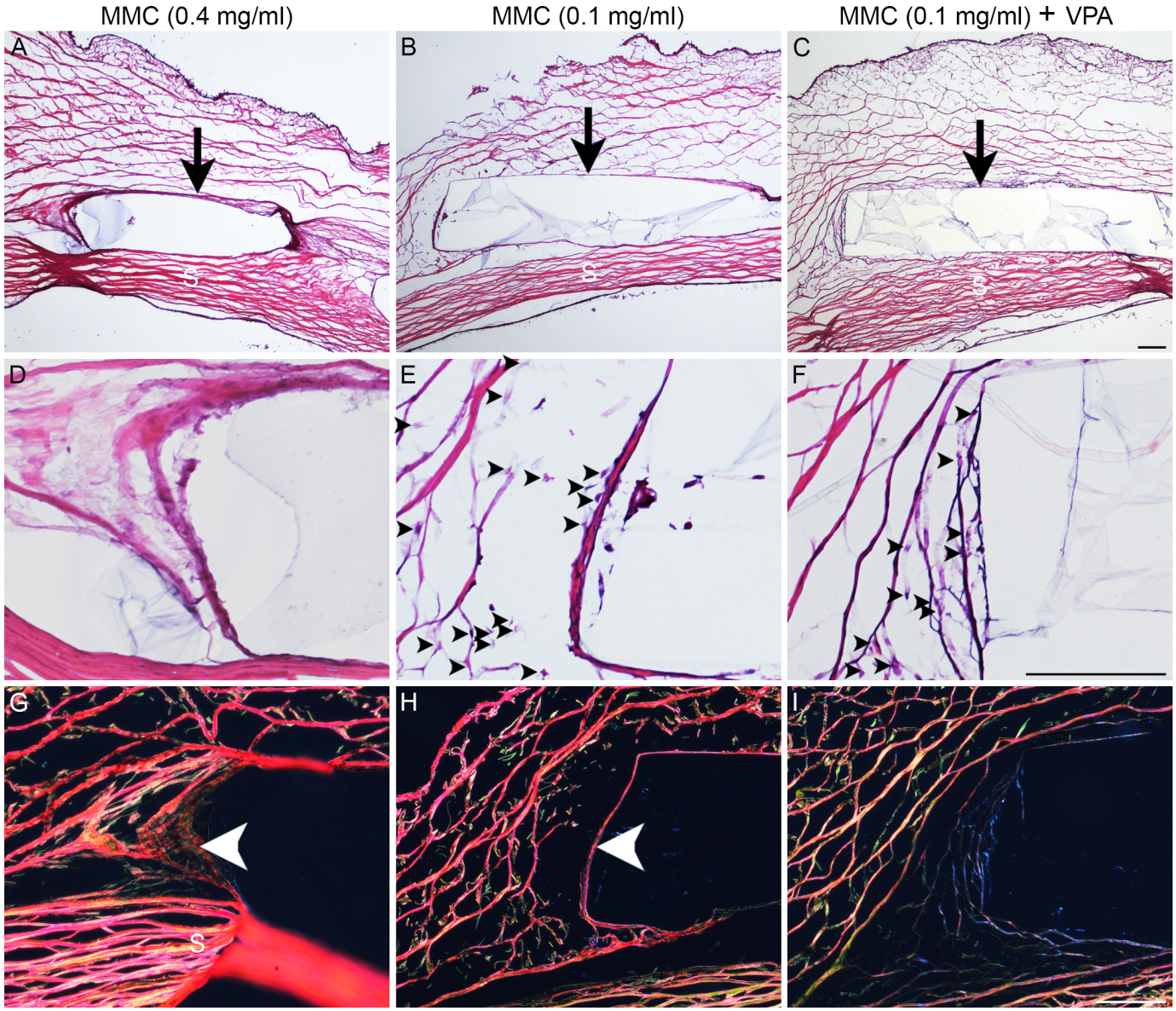

Figure 4. Histochemical evaluation of tissue characteristics surrounding the MicroShunt implant. Rabbit eyes were treated as indicated. Serial frozen sections of the same eye were visualized via staining with H&E (A–F), and picrosirius red (G–I). Panels (A) to (F) were viewed under light microscopy, and (G) to (I) were viewed via polarized microscopy. Panels (D) to (F) are magnified areas of the respective images in (A) to (C). The distal end of the MicroShunt resting in the subconjunctival space above the scleral surface is indicated by a *thin downward arrow*. Examples of spindle-shaped cells with more intensely staining nuclei are indicated by *black arrowheads*. Encapsulation of the lumen at the distal end of the MicroShunt by collagen is indicated by a *white arrowhead*. S, sclera. *Scale bar*: 100 µm.

implanted under the rabbit conjunctiva and Tenon's capsule.[28] In the current study, a thin to extremely thin capsule wall was similarly observed around the MicroShunts under all of the treatment conditions (Figs. 4A–4C, arrows). In all cases, the distal ends of the MicroShunts were seen to rest in the subconjunctival space above the scleral surface, as intended. In the bleb treated with high-dose MMC, the MicroShunt was visualized in the midst of numerous ECM fibers not apparently eliminated by high-dose MMC, but few, if any, cells were detected in the vicinity (Fig. 4D). In the tissue treated with low-dose MMC, spindle-shaped cells, probably corresponding to fibroblasts, were documented close to the distal end of the MicroShunt (Fig. 4E, arrowheads), signifying potential cellular migration into the tube lumen. Cellular presence around the distal end of the implant was similarly observed in the tissue treated with MMC+VPA (Fig. 4F, arrowheads). Further examination via polarized microscopy of picrosirius

red–stained areas around the MicroShunts revealed startling disparities between the thin layer of collagen that clearly enveloped the distal end of the implant in the bleb treated with a low dose of MMC (Fig. 4H, arrowhead), as well as the apparent lack of such a defined collagen shield around the implant opening in the tissue treated with MMC+VPA (Fig. 4I). On the other hand, the high concentrations of fibers surrounding the MicroShunt mouth treated with high-dose MMC suggest a potential risk of blockage by a collagen sheath at the distal end (Fig. 4G, arrowhead). These observations imply that, although high-dose MMC may appear to be most effective in reducing the risk of cellular migration into the implant at the time of evaluation, the risk of encapsulation of the distal opening of the MicroShunt was not eliminated. On the other hand, although cellular survival and migration may not be affected by the combination therapy, the risk of encapsulation appeared to be reduced.

Effects of Combination Therapy on Collagen Fiber Characteristics

Label-free multiphoton imaging of cryosections was next performed to quantify conjunctival stromal collagen characteristics. The green second-harmonic generation (SHG) signals representing fibrillar collagen reiterated the patterns detected by histochemical analyses for the respective treatment conditions (Fig. 5A). Quantitation of the SHG signals using the FibroIndex algorithm revealed that collagen fiber density (CFD), defined as the sum of the SHG pixel intensities within the collagen area, was only significantly reduced in tissues treated with low-dose MMC (1.48-fold; $P = 0.029$) or MMC+VPA (1.83-fold; $P = 0.0018$) but not with high-dose MMC when compared with the unoperated conjunctiva (Fig. 5B). The addition of VPA did not cause significant further CFD reduction compared with low-dose MMC alone. On the other hand, collagen fiber thickness was significantly lower in the bleb treated with high-dose MMC (1.29-fold; $P = 0.021$) or MMC+VPA (1.56-fold; $P = 0.00031$), when compared with the unoperated conjunctiva (Fig. 5C). As treatment with MMC+VPA resulted in significantly thinner fibers compared with treatment with low-dose MMC alone (1.32-fold; $P = 0.040$), the implication is that VPA per sé has the capacity to cause significant reduction in collagen fiber thickness. In terms of mean collagen fiber length, MMC+VPA was the only treatment that resulted in significantly shorter fibers compared with that in the unoperated tissue (1.46-fold; $P = 0.00032$) (Fig. 5D). Mean collagen fiber length in blebs treated with MMC alone, regardless of concentration, was not significantly altered from the unoperated counterpart. Furthermore, we compared the levels of collagen fiber branching by measuring the collagen reticulation index (CRI), which was calculated as a function of collagen length, or the collagen area reticulation density (CARD), which was calculated as a function of collagen area. The presence of VPA caused significantly higher CRI and CARD in the treated blebs compared with all other treatment conditions, including the unoperated counterpart (Figs. 5E, 5F). Incidentally, none of these parameters was significantly different between high- and low-dose MMC. These data suggest that, although high-dose MMC was effective in reducing the thickness of collagen fibers and low-dose MMC was effective in reducing collagen fiber density compared with the unoperated counterpart, the incorporation of VPA in low-dose MMC therapy modified the subconjunctival scar structure in multiple ways through reducing fiber density, thickness, and length while increasing fiber branching in the stromal matrix.

Effects of Combination Therapy on *Vegf* and *Col1a1* Expression

To determine whether the day 28 vascular phenotype was associated with changes in the expression of members of the vascular endothelial growth factor (VEGF) family, we measured the conjunctival expression of *Vegf* mRNAs. *Vegfa* transcripts in the MMC+VPA arm were significantly downregulated from the baseline unoperated level (2.52-fold; $P = 0.019$) (Fig. 6A). As for *Vegfc*, significant downregulation from the unoperated level occurred with high-dose MMC treatment (1.64-fold; $P = 0.011$) but not with low-dose MMC (Fig. 6B). However, the addition of VPA to low-dose MMC caused a significant reduction of *Vegfc* mRNA, down by 1.76-fold relative to the unoperated level (Fig. 6B). On the other hand, *Vegfd* transcripts in the tissues treated with high-dose MMC were not significantly different from the unoperated level but were significantly upregulated in the tissues treated with low-dose MMC (1.44-fold; $P = 0.011$) (Fig. 6C). Combination therapy with VPA significantly reduced *Vegfd* induction by a mean of 2.43-fold ($P = 0.00039$) from the unoperated level (Fig. 6C). At this level, mean *Vegfd* induction was significantly lower compared to that in either high-dose or low-dose MMC monotherapies (Fig. 6C).

We next determined whether the expression of type I collagen was altered in the day 28 postoperative tissues. Of the three conditions, only low-dose MMC monotherapy caused a significant upregula-

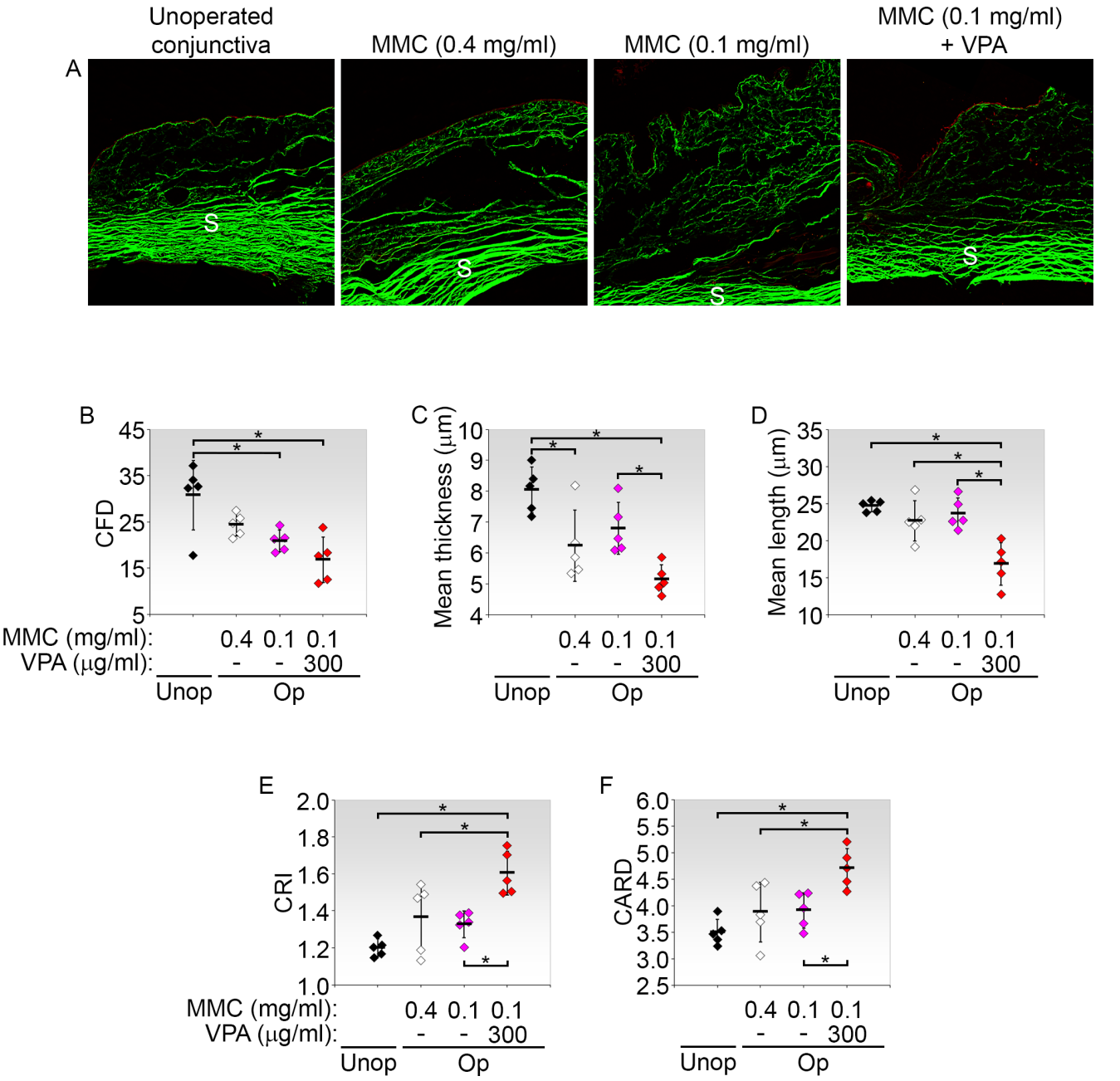

Figure 5. Multiphoton imaging and quantitation of collagen parameters in the day 28 postoperative conjunctivas. Rabbit eyes were treated as indicated. Unoperated normal rabbit conjunctiva is included for comparison. The stain-free cryosections were viewed using multiphoton microscopy. (A) SHG signals (*green*) map the distribution of collagen fibers. S, sclera. SHG signals were quantitated using the FibroIndex algorithm for CFD (B), mean collagen fiber thickness (C), mean collagen fiber length (D), the CRI (E), and CARD (F). Each *symbol* represents one rabbit eye. Values for the mean ± standard deviation per condition ($n = 5$) are indicated by the *horizontal bars*. *$P < 0.05$, Bonferroni adjusted.

tion of *Col1a1* mRNA expression, by 2.91-fold ($P = 0.0010$) when compared with unoperated tissue levels (Fig. 6D). In contrast, the incorporation of VPA effectively suppressed *Col1a1* mRNA induction from the baseline unoperated level, as did high-dose MMC. At the protein level, the large scatter in COL1A1 levels in the high-dose MMC arm suggests great variability in COL1A1 protein content among individual tissues under this condition (Fig. 6E). In comparison, there was less deviation in COL1A1 protein levels in the blebs treated with low-dose MMC, and the most stable and consistent COL1A1 protein levels (smallest

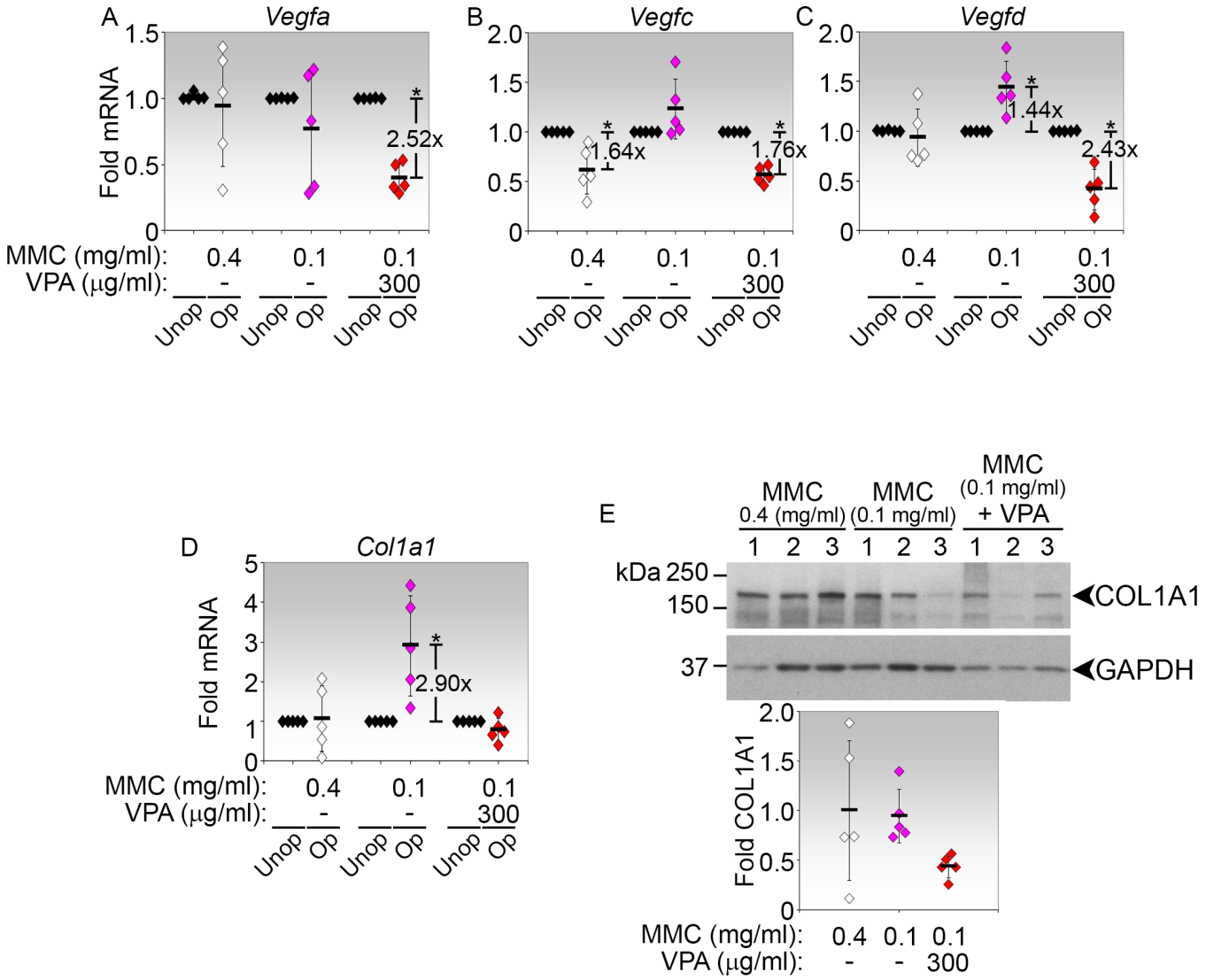

Figure 6. *Vegf* and *Col1a1* expression in the day 28 postoperative conjunctivas. Rabbit eyes were treated as indicated. Conjunctival tissues from both contralateral unoperated and operated eyes were harvested and subjected to analyses by qPCR for *Vegfa* (A), *Vegfc* (B), *Vegfd* (C), and *Col1a1* (D) transcripts. Values shown were calculated as fold changes from contralateral unoperated levels whose values are represented by *black diamonds*. Each symbol represents one rabbit eye. Values for the mean fold change ± standard deviation per condition ($n = 5$) are indicated by the *horizontal bars*. The fold differences in mean expression between the indicated conditions, where significant, are also shown. *$P < 0.05$, Bonferroni-adjusted. (E) Postoperative tissues were harvested and subjected to analyses by immunoblotting with COL1A1 antibody. (*Top*) Representative blots showing three samples for each condition probed with COL1A1 or GAPDH antibody. (*Bottom*) Densitometric analyses of COL1A1 expression, normalized to GAPDH. Each value represents the fold of normalized COL1A1 signal intensity relative to the mean signal intensity measured in the high-dose MMC arm. Values for the mean fold ± standard deviation per condition ($n = 5$) are indicated by the horizontal bars.

standard deviation) were measured in the blebs treated with MMC+VPA (Fig. 6E). Although not statistically significant, the addition of VPA caused a 2.15-fold reduction in the mean COL1A1 protein level relative to low-dose MMC monotherapy alone (Fig. 6E). Taken together, the incorporation of VPA to low-dose MMC not only effectively reduced the mRNA of all three *Vegf* members to below the baseline unoperated levels but also suppressed the induction of *Col1a1* mRNA with an efficacy similar to that of high-dose MMC. The addition of VPA further promised greater consistency in the reduction of COL1A1 protein content in the treated bleb.

Discussion

We reveal in this study that the combination therapy of low-dose MMC and VPA was effective in protect-

ing the postoperative vasculature that was overtly disrupted by high-dose MMC. Importantly, not only was the effectiveness of this combination therapy in reducing molecular expression of type I collagen comparable to that of high-dose MMC, but it also did so in a more consistent manner and caused alterations in collagen organization synonymous with weaker scars. Moreover, the risk of MicroShunt encapsulation was also apparently decreased. This combination therapy is therefore expected to reduce the risk of adverse side effects while achieving the same and potentially improved anti-scarring results as high-dose MMC monotherapy.

High-dose MMC is associated with a high incidence of bleb avascularity. This has been well documented in patients[10] and reiterated in animal models, including the mouse model of conjunctival scarring[9] and rabbit model of glaucoma filtration surgery.[29] MMC is known to be highly toxic to capillary endothelial cells.[30] As capillary endothelial cells are a rich source of VEGF,[31] the depletion of these cells in turn inhibits angiogenesis during wound healing, resulting in the progressive development of a pale, avascular bleb. Indeed, progressive avascularity with high-dose MMC was observed in this study, corroborating similar observations in patients.[10] Avascular blebs, especially those covering large areas, are prone to spontaneous leakage and transconjunctival oozing.[10] Hence, a long-lasting healthy bleb will preferably retain some vascularity while avoiding the excessive vascularization that has frequently been associated with surgical failure.[32] Here, we show that the application of low-dose MMC reduced bleb avascularity compared with high-dose MMC, but the addition of VPA went further by seemingly supporting the survival of the vasculature without an apparent increase in vascularization. Indeed, VPA is known to activate cell survival signaling pathways,[33] provide cytoprotective effects in lethal hemorrhage,[34] and preserve endothelial function in a model of severe traumatic shock.[35] At the same time, VPA has been noted for its capacity to suppress multiple pathways of angiogenesis.[36] This study further reveals that the addition of VPA can lead to significant reductions of all three known *Vegf* members in the rabbit conjunctiva. *Vegfa* is a well-established regulator of angiogenesis, but both *Vegfc*[37] and *Vegfd*[38] are emerging as potent angiogenic factors in pathological angiogenesis. Moreover, these factors are known to regulate blood vessel size,[38,39] which may account for the more refined vessels seen in the blebs treated with combination therapy. We further speculate that the VPA effect on blood vessel dimensions may also be contributed to by reduced collagen deposition, as vessel size was demonstrated to positively correlate with collagen density in both in vivo and in vitro experimental studies.[40]

The detection of a high incidence and density of microcystic spaces in the bleb epithelium and stroma by slit-lamp biomicroscopy and in vivo confocal microscopy has been shown to correlate significantly with good filtering bleb function.[41–43] In agreement with the human response to MMC,[44,45] the rabbit bleb treated with high-dose MMC also presented with numerous microcysts that suggest good filtration function. The clustering distribution of epithelial microcysts detected with high-dose MMC was similarly observed in patients treated with MMC.[46] As treatment with low-dose MMC, alone or combined with VPA, clearly resulted in fewer microcysts in the epithelium and conspicuously smaller microcysts in the stroma, these treatments may be deemed less effective than high-dose MMC in supporting a good functional bleb. However, microcyst detection, as a sign of drainage capacity, is only one gauge of bleb functionality. Weak scars may allow filtration to occur without the need for physically detectable microcysts. In the case of MIGS, encapsulation of the MicroShunt is also an important consideration. Hence, other measures directly related to the level of scarring after therapeutic treatment warrant detailed evaluation

Consistent with observations in patients treated with high-dose MMC,[47–50] large acellular and avascular spaces that reflect MMC toxicity were seen in similarly treated rabbit eyes. However, mature collagen fibers, likely remnants of the original pre-surgery network spared from MMC toxicity, as well as cells resembling spindle-shaped fibroblasts, were conspicuously present in the periphery and boundaries of this space. Hence, disparities in MMC exposure areas between treated eyes will likely result in variability in effects, particularly with respect to collagen quantity, thus accounting for the large deviation in type I collagen protein levels measured. Furthermore, the localized and incomplete coverage of the subconjunctiva by high-dose MMC activity may imply that scar formation is still possible. Indeed, the potential encroachment of collagen fibers toward the distal end of the MicroShunt may be a sign of increasing scarring activity. Nonetheless, at the time of examination, we did not observe cells in the vicinity of the distal end of the MicroShunt, which suggests that cellular activity was still effectively controlled by the high-dose MMC.

Although bleb survival was noted with all treatments, the long-term risk of failure may be highest in the bleb treated with low-dose MMC monother-

apy. The obvious cellular presence, particularly around the distal end of the MicroShunt, was an ominous sign for the potential risk of scarring. More importantly, the tissue was inundated with numerous apparently immature collagen fibers, indicating that active collagen deposition was still occurring at 1 month post-surgery. This was corroborated by the significant elevation of *Col1a1* mRNA induction in tissues treated with low-dose MMC at this time point. The addition of VPA to low-dose MMC therapy effectively blocked *Col1a1* mRNA induction. This implies that collagen production was paused or maintained at steady-state levels by VPA, as substantiated by the mature appearance of the fibers observed by histochemical examination. The suppression of collagen production in the MMC+VPA bleb further correlated with visibly less MicroShunt encapsulation, particularly toward the distal end opening that is critical for drainage. The impact of VPA on conjunctival collagen production is consistent with our previous findings in both mouse and rabbit models.[22,23] On addition to inhibiting collagen synthesis, the addition of VPA altered the collagen matrix dramatically, with a predominance of significantly thinner and shorter fibers compared with that treated with low-dose MMC alone. Notably, the deposition of thinner fibers was another consistent observation associated with VPA treatment.[23] The implication of the increased reticulation from VPA treatment on tissue function is uncertain. We do not anticipate that tissue stiffness associated with collagen reticulation will be increased, as this feature was concurrent with reduced collagen density together with thinner and shorter fibers.

Taken together, this study has demonstrated that VPA modulates collagen deposition in both quantity and quality, with all attributes tending toward that of a weaker postoperative scar. Moreover, our data suggest that, although high-dose MMC via sponge application may reduce local scar formation by drastic devastation of the subconjunctival matrix, cells, and vasculature, inhibition is unlikely to be complete and, when coupled with adverse effects arising from the tissue damage, surgical success will be compromised and cannot be guaranteed. On the other hand, low-dose MMC demonstrated much less toxicity with respect to cells and vascularity but was utterly ineffective in reducing collagen production. As a reflection of the distinct mechanisms afforded by the respective drugs, the addition of VPA to low-dose MMC not only provided for the deficiency of the latter in controlling collagen production but also protected the vasculature and further modified the scar structure to one that may favor filtration. This study therefore suggests that a combination of low-dose MMC and VPA may be a viable clinical replacement for high-dose MMC for achieving improved and safer long-term outcomes for GFS and MIGS.

Acknowledgments

The authors thank Gideon Ho (HistoIndex Pte. Ltd.) and Serene Lek (Clinnovate Health Pte. Ltd.) for their help in supporting and coordinating the multiphoton imaging and quantitative analyses.

Supported by a grant from the Singapore National Eye Centre Health Research Endowment Fund (HREF0218-3), by a Clinician Scientist Award Grant (NMRC/CSA-SI/0001/2015), and by the A*STAR Industry Alignment Fund–Industry Collaboration Projects (I1601E0008). Animal studies were partially funded by a SERI core grant (NMRC/CG/015/2013) administered by the Singapore Ministry of Health's National Medical Research Council. Santen Pharmaceutical provided the PreserFlo implants.

Disclosure: **L.F. Seet**, None; **Z.L. Yap**, None; **S.W.L Chu**, None; **L.Z. Toh**, None; **F.I. Ibrahim**, None; **X. Teng**, None; **T.T. Wong**, None

* LFS and ZLY contributed equally to this work.

References

1. Heijl A, Leske MC, Bengtsson B, Hyman L, Hussein M, Early Manifest Glaucoma Trial Group. Reduction of intraocular pressure and glaucoma progression: results from the Early Manifest Glaucoma Trial. *Arch Ophthalmol.* 2002;120:1268–1279.
2. Gedde SJ, Schiffman JC, Feuer WJ, et al. Treatment outcomes in the tube versus trabeculectomy (TVT) study after five years of follow-up. *Am J Ophthalmol*. 2012;153:789–803.e2.
3. Caprioli J, Kim JH, Friedman DS, et al. Special commentary: supporting innovation for safe and effective minimally invasive glaucoma surgery: summary of a Joint Meeting of the American Glaucoma Society and the Food and Drug Administration, Washington, DC, February 26, 2014. *Ophthalmology*. 2015;122:1795–1801.
4. Pinchuk L, Riss I, Batlle JF, et al. The development of a micro-shunt made from poly(styrene-block-

isobutylene-block-styrene) to treat glaucoma. *J Biomed Mater Res B Appl Biomater*. 2017;105:211–221.
5. Beckers HJM, Pinchuk L. Minimally invasive glaucoma surgery with a new ab-externo subconjunctival bypass - current status and review of literature. *Eur Ophthalmic Rev*. 2019;13:27–30.
6. Crowston JG, Akbar AN, Constable PH, Occleston NL, Daniels JT, Khaw PT. Antimetabolite-induced apoptosis in Tenon's capsule fibroblasts. *Invest Ophthalmol Vis Sci*. 1998;39:449–454.
7. Chen CW. Enhanced intraocular pressure controlling effectiveness of trabeculectomy by local application of mitomycin C. *Trans Asia-Pacific Acad Ophthalmol*. 1983;9:172–177.
8. Bell K, de Padua Soares Bezerra B, Mofokeng M, et al. Learning from the past: mitomycin C use in trabeculectomy and its application in bleb-forming minimally invasive glaucoma surgery. *Surv Ophthalmol*. 2021;66:109–123.
9. Seet LF, Lee WS, Su R, Finger SN, Crowston JG, Wong TT. Validation of the glaucoma filtration surgical mouse model for antifibrotic drug evaluation. *Mol Med*. 2011;17:557–567.
10. Anand N, Arora S, Clowes M. Mitomycin C augmented glaucoma surgery: evolution of filtering bleb avascularity, transconjunctival oozing, and leaks. *Br J Ophthalmol*. 2006;90:175–180.
11. Higginbotham EJ, Stevens RK, Musch DC, et al. Bleb-related endophthalmitis after trabeculectomy with mitomycin C. *Ophthalmology*. 1996;103:650–656.
12. Occleston NL, Daniels JT, Tarnuzzer RW, et al. Single exposures to antiproliferatives: long-term effects on ocular fibroblast wound-healing behavior. *Invest Ophthalmol Vis Sci*. 1997;38:1998–2007.
13. Seet LF, Su R, Toh LZ, Wong TT. In vitro analyses of the anti-fibrotic effect of SPARC silencing in human Tenon's fibroblasts: comparisons with mitomycin C. *J Cell Mol Med*. 2012;16:1245–1259.
14. Law SK, Modjtahedi SP, Mansury A, Caprioli J. Intermediate term comparison of trabeculectomy with intraoperative mitomycin-C between Asian American and Caucasian glaucoma patients: a case-controlled comparison. *Eye (Lond)*. 2007;21:71–78.
15. Sihota R, Angmo D, Chandra A, Gupta V, Sharma A, Pandey RM. Evaluating the long-term efficacy of short-duration 0.1 mg/ml and 0.2 mg/ml MMC in primary trabeculectomy for primary adult glaucoma. *Graefes Arch Clin Exp Ophthalmol*. 2015;253:1153–1159.
16. Foo VHX, Htoon HM, Welsbie DS, Perera SA. Aqueous shunts with mitomycin C versus aqueous shunts alone for glaucoma. *Cochrane Database Syst Rev*. 2019;4:CD011875.
17. Holló G. Wound healing and glaucoma surgery: modulating the scarring process with conventional antimetabolites and new molecules. *Dev Ophthalmol*. 2017;59:80–89.
18. Lee JJ, Park KH, Youn DH. The effect of low-and high-dose adjunctive mitomycin C in trabeculectomy. *Korean J Ophthalmol*. 1996;10:42–47.
19. Alwitry A, Abedin A, Patel V, Moodie J, Rotchford A, King AJ. Primary low-risk trabeculectomy augmented with low-dose mitomycin-C. *Eur J Ophthalmol*. 2009;19:971–976.
20. Al Habash A, Aljasim LA, Owaidhah O, Edward DP. A review of the efficacy of mitomycin C in glaucoma filtration surgery. *Clin Ophthalmol*. 2015;9:1945–1951.
21. Khan S, Ahirwar K, Jena G. Anti-fibrotic effects of valproic acid: role of HDAC inhibition and associated mechanisms. *Epigenomics*. 2016;8:1087–1101.
22. Seet LF, Toh LZ, Finger SN, Chu SW, Stefanovic B, Wong TT. Valproic acid suppresses collagen by selective regulation of Smads in conjunctival fibrosis. *J Mol Med (Berl)*. 2016;94:321–334.
23. Yap ZL, Seet LF, Chu S, Toh LZ, Ibrahim F, Wong TT. The effect of valproic acid on functional bleb morphology in a rabbit model of minimally invasive surgery [published online ahead of print July 15, 2021]. *Br J Ophthalmol*, https://doi.org/10.1136/bjophthalmol-2020-318691.
24. Seet LF, Chu SWL, Teng X, Toh LZ, Wong TT. Assessment of progressive alterations in collagen organization in the postoperative conjunctiva by multiphoton microscopy. *Biomed Opt Express*. 2020;11:6495–6515.
25. Andersen CL, Jensen JL, Ørntoft TF. Normalization of real-time quantitative reverse transcription-PCR data: a model-based variance estimation approach to identify genes suited for normalization, applied to bladder and colon cancer data sets. *Cancer Res*. 2004;64:5245–5250.
26. Seet LF, Finger SN, Chu SW, Toh LZ, Wong TT. Novel insight into the inflammatory and cellular responses following experimental glaucoma surgery: a roadmap for inhibiting fibrosis. *Curr Mol Med*. 2013;13:911–928.
27. Pierad GE. Sirius red polarization method is useful to visualize the organization of connective tissues but not the molecular composition of their fibrous polymers. *Matrix*. 1989;9:68–71.
28. Acosta AC, Espana EM, Yamamoto H, et al. A newly designed glaucoma drainage implant made of poly(styrene-b-isobutylene-b-styrene): biocom-

patibility and function in normal rabbit eyes. *Arch Ophthalmol*. 2006;124:1742–1749.
29. Wong TT, Mead AL, Khaw PT. Prolonged antiscarring effects of ilomastat and MMC after experimental glaucoma filtration surgery. *Invest Ophthalmol Vis Sci*. 2005;46:2018–2022.
30. Smith S, D'Amore PA, Dreyer EB. Comparative toxicity of mitomycin C and 5-fluorouracil in vitro. *Am J Ophthalmol*. 1994;118:332–337.
31. Seghezzi G, Patel S, Ren CJ, et al. Fibroblast growth factor-2 (FGF-2) induces vascular endothelial growth factor (VEGF) expression in the endothelial cells of forming capillaries: an autocrine mechanism contributing to angiogenesis. *J Cell Biol*. 1998;141:1659–1673.
32. Grover DS, Kornmann HL, Fellman RL. Historical considerations and innovations in the perioperative use of mitomycin C for glaucoma filtration surgery and bleb revisions. *J Glaucoma*. 2020;29:226–235.
33. De Sarno P, Li X, Jope RS. Regulation of Akt and glycogen synthase kinase-3β phosphorylation by sodium valproate and lithium. *Neuropharmacology*. 2002;43:1158–1164.
34. Gonzales ER, Chen H, Munuve RM, Mehrani T, Nadel A, Koustova E. Hepatoprotection and lethality rescue by histone deacetylase inhibitor valproic acid in fatal hemorrhagic shock. *J Trauma*. 2008;65:554–565.
35. Causey MW, Salgar S, Singh N, Martin M, Stallings JD. Valproic acid reversed pathologic endothelial cell gene expression profile associated with ischemia-reperfusion injury in a swine hemorrhagic shock model. *J Vasc Surg*. 2012;55:1096–1103.e51.
36. Michaelis M, Michaelis UR, Fleming I, et al. Valproic acid inhibits angiogenesis in vitro and in vivo. *Mol Pharmacol*. 2004;65:520–527.
37. Singh NK, Kotla S, Kumar R, Rao GN. Cyclic AMP response element binding protein mediates pathological retinal neovascularization via modulating DLL4-NOTCH1 signaling. *EBioMed*. 2015;2:1767–1784.
38. Rissanen TT, Markkanen JE, Gruchala M, et al. VEGF-D is the strongest angiogenic and lymphangiogenic effector among VEGFs delivered into skeletal muscle via adenoviruses. *Circ Res*. 2003;92:1098–1106.
39. Nakatsu MN, Sainson RC, Pérez-del-Pulgar S, et al. VEGF(121) and VEGF(165) regulate blood vessel diameter through vascular endothelial growth factor receptor 2 in an in vitro angiogenesis model. *Lab Invest*. 2003;83:1873–1885.
40. Critser PJ, Kreger ST, Voytik-Harbin SL, Yoder MC. Collagen matrix physical properties modulate endothelial colony forming cell-derived vessels in vivo. *Microvasc Res*. 2010;80:23–30.
41. Addicks EM, Quigley HA, Green WR, Robin AL. Histologic characteristics of filtering blebs in glaucomatous eyes. *Arch Ophthalmol*. 1983;101:795–798.
42. Messmer EM, Zapp DM, Mackert MJ, Thiel M, Kampik A. In vivo confocal microscopy of filtering blebs after trabeculectomy. *Arch Ophthalmol*. 2006;124:1095–1103.
43. Güven Yılmaz S, Değirmenci C, Palamar M, Yağcı A. Evaluation of filtering bleb function after trabeculectomy with mitomycin C using biomicroscopy, anterior segment optical coherence tomography and in vivo confocal microscopy. *Turk J Ophthalmol*. 2015;45:132–137.
44. Labbé A, Dupas B, Hamard P, Baudouin C. In vivo confocal microscopy study of blebs after filtering surgery. *Ophthalmology*. 2005;112:1979–1986.
45. Guthoff R, Klink T, Schlunck G, Grehn F. In vivo confocal microscopy of failing and functioning filtering blebs: results and clinical correlations. *J Glaucoma*. 2006;15:552–558.
46. Ciancaglini M, Carpineto P, Agnifili L, et al. Conjunctival characteristics in primary open-angle glaucoma and modifications induced by trabeculectomy with mitomycin C: an in vivo confocal microscopy study. *Br J Ophthalmol*. 2009;93:1204–1209.
47. Shields MB, Scroggs MW, Sloop CM, Simmons RB. Clinical and histopathologic observations concerning hypotony after trabeculectomy with adjunctive mitomycin C. *Am J Ophthalmol*. 1993;116:673–683.
48. Hutchinson AK, Grossniklaus HE, Brown RH, McManus PE, Bradley CK. Clinicopathologic features of excised mitomycin filtering blebs. *Arch Ophthalmol*. 1994;112:74–79.
49. Nuyts RM, Felten PC, Pels E, et al. Histopathologic effects of mitomycin C after trabeculectomy in human glaucomatous eyes with persistent hypotony. *Am J Ophthalmol*. 1994;118:225–237.
50. Mietz H, Arnold G, Kirchhof B, Diestelhorst M, Krieglstein GK. Histopathology of episcleral fibrosis after trabeculectomy with and without mitomycin C. *Graefes Arch Clin Exp Ophthalmol*. 1996;234:364–368.